

# bradscholars

## Analytical modelling and electrochemical impedance spectroscopy (EIS) to evaluate influence of corrosion product on solution resistance

Item Type	Article
Authors	Ikani, N.;Pu, Jaan H.;Cooke, Kavian O.
Citation	Ikani N, Pu JH and Cooke K (2024) Analytical modelling and electrochemical impedance spectroscopy (EIS) to evaluate influence of corrosion product on solution resistance. Powder Technology. 433: 119252.
DOI	<a href="https://doi.org/10.1016/j.powtec.2023.119252">https://doi.org/10.1016/j.powtec.2023.119252</a>
Publisher	Elsevier
Rights	© 2023 The Authors. Published by Elsevier B.V. This is an open access article under the CC BY license ( <a href="http://creativecommons.org/licenses/by/4.0/">http://creativecommons.org/licenses/by/4.0/</a> ).
Download date	2026-04-19 02:24:48
Link to Item	<a href="http://hdl.handle.net/10454/20070">http://hdl.handle.net/10454/20070</a>



# Analytical modelling and electrochemical impedance spectroscopy (EIS) to evaluate influence of corrosion product on solution resistance

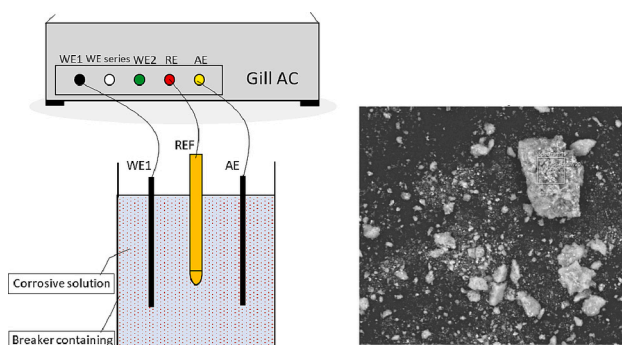
Nima Ikani, Jaan H. Pu<sup>\*</sup>, Kavian Cooke

Faculty of Engineering and Informatics, University of Bradford, Bradford DB7 1DP, UK

## HIGHLIGHTS

- Proposed analytical model for relation between solution and corrosion particles.
- Experiments for the influence of solution resistance across varying concentrations.
- This research addresses concern in both industrial and environmental contexts.

## GRAPHICAL ABSTRACT



## ARTICLE INFO

### Keywords:

Electrochemical impedance spectroscopy (EIS)  
Density  
Corrosion  
Impedance  
Resistance  
Conductivity

## ABSTRACT

Electrochemical impedance spectroscopy (EIS) is a technique used to evaluate the electrochemical behavior of metallic materials in different environments. In this study, a mathematical model has been developed to analyse the relationship between solution resistance and concentration conductive-corrosion products ( $\text{Fe}_2\text{O}_3$ ) of metallic corroded materials. This model has been designed as a part of an experimental series to use EIS as a tool for mapping the spatial distribution of corrosion by-product from bridge, in order to evaluate the impact of conductive-corrosion on the properties of the solution. The influence of  $\text{Fe}_2\text{O}_3$  on the solution resistance at varying concentrations, has been modelled. Repetitive electrochemical tests were conducted to investigate the relationship between the impedance and concentration in three different concentrations of corrosion by-product. Nyquist and Bode's graphs have been used to quantitatively analyse the EIS data. The implementation of the proposed mathematical model can quantify the solution resistance based on the mass of presented particles, and provide significant efficiency and methodological advancement over EIS technique. The experimental outcomes show a clear link between solution resistance and iron oxide concentration within the solution which is consistent with the model's finding.

<sup>\*</sup> Corresponding author.

E-mail addresses: [n.ikani@bradford.ac.uk](mailto:n.ikani@bradford.ac.uk) (N. Ikani), [j.h.pu1@bradford.ac.uk](mailto:j.h.pu1@bradford.ac.uk) (J.H. Pu), [k.cooke1@bradford.ac.uk](mailto:k.cooke1@bradford.ac.uk) (K. Cooke).

<https://doi.org/10.1016/j.powtec.2023.119252>

Received 27 August 2023; Received in revised form 18 November 2023; Accepted 4 December 2023

Available online 12 December 2023

0032-5910/© 2023 The Authors. Published by Elsevier B.V. This is an open access article under the CC BY license (<http://creativecommons.org/licenses/by/4.0/>).

## 1. Introduction

The phenomenon of corrosion refers to a progressive degradation of a metal's properties due to a chemical reaction between the metal and its surrounding environment [63]. Conversely, a refined metal may exhibit enhanced chemical stability over an extended time when it is exposed to air and water which act to reduce further reactivity of metal's surface with the environment [39,72]. The tendency and the corresponding potential of a material to be corroded are determined by a variety of factors. These factors include the density and concentration of material in the immediate environment [5,73], temperature [23,31,35,44,75], different pH conditions [2,15,46,51,52], electrochemical properties [58], and electrochemical potential [65]. Since corrosion is fundamentally an electrochemical (EC) process, Electrochemical Impedance Spectroscopy (EIS) has been recognised as one of the most reliable quantitative technique to examine the mechanism of electrochemical reactions at interfaces and diagnose corrosion [42,67,69,70]. Through the characterisation of ionic resistance in metals, EIS measurements provide reliable data within a short testing period that can be evaluated to predict its long-term corrosion performance [64]. In particular, the EIS is used to investigate interfacial reaction mechanisms and to find the transfer function between currents and potentials based on the impedance of the electrochemical system, and can be determined as a function of frequency. The EIS measurement becomes a powerful technique due to its workability using an alternating current signal of relatively small amplitude. This allows a detailed examination of the dynamic process, the progressive evolution of electrochemical reactions, and the transport processes during the formation of corrosion product [28,54].

Numerous investigations have been conducted on the conductivity and resistance of the electrolyte, as they play critical role in electrochemical techniques due to their ability on detection of corrosion [1,6,7,45]. Alexander and Orazem [1] used a combination of experiments and simulations to assess the feasibility of applying the indirect impedance technique to detect corrosion of steel in post-tensioned tendons used in the construction of segmental bridge. Their EIS data can be correlated with a number of key physical properties, including diffusion, reaction rates, and microstructural characteristics [1,12]. In this respect, Ciucci [7] further employed the EIS technique and introduced the concept of the Distribution of Relaxation Times (DRT) to estimate relaxation characteristics of electrochemical systems. On the other hand, Holm et al. [20] further investigated the convective-diffusion problem under alternating current conditions and the behavior of microelectrodes in thin-layer cells.

Finite element analysis (FEA) has been effectively employed to calculate impedance, which has been used to confirm the flow rates in microfluidic flow cells. The results, however, indicate that they may not be applicable to scenarios involving low flow rates or specific channel dimensions. According to Nasser-Eddine et al. [57], in order to overcome challenges related to incomplete spectra, the chronopotentiometry should be combined with EIS. In Huang [25] study, new models are presented that better addressed complex scenarios of EIS's electrochemical system. They have revisited the limitations in the original Warburg impedance model by expanding boundary conditions and incorporating diffusion impedance in porous materials and fractal geometries.

Advance methods have also been suggested to develop new type of electrode cell design for measuring solution conductivity [3], and also to study the impact of the capacitive nature of conductivity cell where the relationship between electrochemical parameters has been explored [14]. Murphy and Caudle [56] have first presented a mathematical theory for electrochemical cells containing porous cation and anion-responsive electrodes. A good agreement has been demonstrated between the theoretical predictions and experimental observations for concentration versus time profile as a function of physical parameters used in data analysis for cell concentration changes. More recently, Huang et al. [26] focused on investigation on physics-based models to enhance the

understanding of the complexities of transport phenomena and coupled interfacial reactions within porous electrodes. Following from theoretical findings, they developed a framework for extending the Levie model by incorporating novel physico-chemical processes that treat structural effects in porous electrodes. By using the galvanostatic intermittent titration technique (GITT), Jia et al. [34] advanced the understanding of chemical diffusion coefficients. Their study focused on the transport of charged species in electrochemical reactions by using voltage relaxation, charge-transfer, and transient measurements. Further, using the GITT technique, He et al. [19] introduced the concept of charge-transfer resistance's relevance in the high-frequency region. In their findings, impedance measurements are responsible to determine the electroactive ion surface concentration at the anode. Furthermore, their study highlighted limitations in specific assumptions, such as the bulk concentration of electroactive ions, prior to an experiment. Some studies have utilised the theoretical behavior of EIS, which is typically based on the Nernst-Planck flux equations that are commonly used in ion transport modelling, along with the Poisson equation, as a numerical simulation of ion-selective membrane electrodes for ionic sites with steady-state potentials and impedance spectra [17,19,36]. However, those system's analytical solution was only workable under idealised and steady-state conditions [33].

Corrosion of coastal structures is usually occurring in slow rate, in which components are typically susceptible to non-uniform corrosion, for example, non-uniform corrosion of bridge piers in the marine environment [9,29,71]. A majority of the studies related to the corrosion behavior were conducted on aggressive mediums such as concentrated acids, chlorides, and oxidizers [4,24,48,49,59,60,68]. There are also several studies investigated the corrosion of steel rebar and bridge pier in marine environment and their behavior including cracking and spalling generation in the concrete cover [13,22,43,66,74]. Duarte et al. [11] presented a method for effectively applying EIS to the corrosion of steel rebar in concrete, emphasizing structural integrity. By integrating advance simulations, their study critically examined and refined previous methodologies. Hoshi et al. [21] further suggested an innovative approach of utilising EIS to enhance the accuracy of corrosion assessments by identifying the integrity of steel rebar within concrete structures. The effectiveness of their technique is based on the incorporation of the Stern-Geary equation.

On the other hand, Colla et al. [8] presented experimental results on water-based nanofluids containing iron oxide in concentrations ranging in mass, which included measurements of thermal conductivity and dynamic viscosity. They found that the effects of temperature and nanoparticle concentration on viscosity were related to Newtonian behavior with respect to water. Su et al. [76] proposed a theoretical approach to determine the conductivity of electrolytic solution using sine waveform voltage as a triggering signal in a two-electrode system. Despite electrode polarisation and capacitance between electrodes which can cause negative influence on the measurement accuracy, it is proven to be theoretical possible to deduce the resistance of electrolytic solution on the basis of analysing the cell's complex impedance, before considering the conductivity of electrolytic solution.

After summarising the research field and identifying its gap, a mathematical model has been developed in this study to analyse the relationship between solution resistance and concentration conductive-corrosion products ( $\text{Fe}_2\text{O}_3$ ) of metallic corroded materials. The proposed model has been designed as part of an experimental series to use EIS as a tool for mapping the spatial distribution of corrosion by-product from bridge and to evaluate the impact of conductive-corrosion on the properties of the solution. By using EIS, this work aims to investigate the electrochemical behavior of conductive corrosion by-products ( $\text{Fe}_2\text{O}_3$ ) in static water that are rarely investigated as discussed in afore literature reviewing. More specifically, this paper provides a mathematical theory about the amount of insoluble particles (in concentration) that affects the electrical resistivity of solutions. By utilising particle mass and concentration as model variables, the analytical model has the

capability to practically estimate the solution's conductivity and resistance in a much shorter timeframe compared to the conventional EIS technique, in which its good agreement to the experiment result from EIS has also been recorded here. The utilised samples have been collected from metallic materials subjected to corrosion in flowing water which is commonly emitted from pier bridge structures exposed to different environmental conditions. It was subsequently dried for the analysis in this study. The study outcomes proved that the predicted change in solution resistivity was in agreement with the observations in the EIS experiment.

## 2. Materials and methods

### 2.1. Experiment setup

The experiments were performed at the University of Bradford's Mechanical Laboratory, UK, using the Atmospheric Corrosion Monitor ACM instrument (Model Gill AC). It is equipped with Electrochemical Impedance Spectroscopy (EIS) technique with a frequency range of 0.004 Hz to 950 Hz. It was evaluated with an amplitude of 32 mV RMS. A total of 150 readings were collected for each test over period of 105 min. The iron oxide ( $Fe_2O_3$ ) particles were dissolved into 900 ml of distilled water at a temperature of 15 degrees centigrade to form the studied solution. The experimental framework contained three distinct tests, with the respective concentrations detailed in Table 1. Before the tests, a magnetic bar rotating at 200 rpm was applied to the solutions for 10 min to ensure uniform suspended particle distribution for increasing its contribution to conductivity.

Fig. 1 shows a schematic representation of the experimental three-electrode cell setup utilised for EIS measurements. This system consisting of a working electrode (WE) made of 440UNC Mild Steel, an auxiliary electrode (AE) represented by a Platinum Band, and a Saturated Calomel electrode for reference electrode (RE). The test was conducted in a breaker container, which does not interfere with the transfer of electrons during testing.

### 2.2. Particles analysis

Scanning Electron Microscopy (SEM) analysis of the iron oxide particles was conducted using an Oxford FEI microscope to determine the morphology and distribution of different elements in the iron oxide sample, along with the detailed surface structure shown in Fig. 2 (the analysis method can be referred to Kulkarni and Lokhande [37], Lan et al. [38]). A Back-Scattered Electron (BSE) was used to determine the distribution of different elements in the sample. Further, Fig. 2 shows the compound's Energy-Dispersive X-ray Spectroscopy (EDS) map, and it confirms Fe and O as main elements. The SEM micrograph also reveals a diversity in particle sizes, ranging from sub-micron dimensions to larger agglomerates. However, the alteration in conductivity remains independent of the particle size (as also suggested by Rong and Feng [62]).

The particle composition and concentration measurement of the elements deduced from SEM analysis are presented in Table 2. As instructed in literature, within the temperature range tested,  $FeO$ ,  $Fe_2O_3$  or  $Fe_3O_4$  is possible. However, the EDS results confirm the particles are likely to be  $Fe_2O_3$ .

**Table 1**  
Solution composition used in the experiment.

Test	Distilled water (ml)	$Fe_2O_3$ Concentration (g)
1	900	0.1
2	900	0.2
3	900	0.5

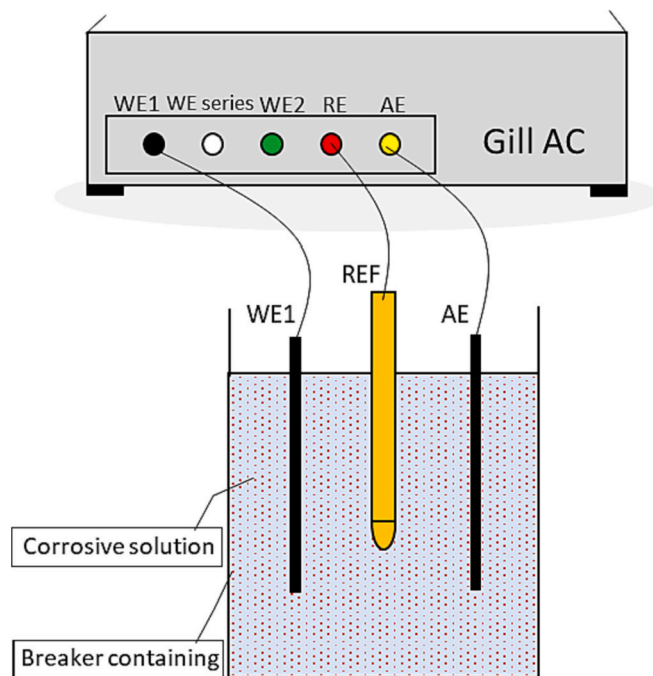


Fig. 1. Electrochemical (EC) test setup using a three-electrode cell.

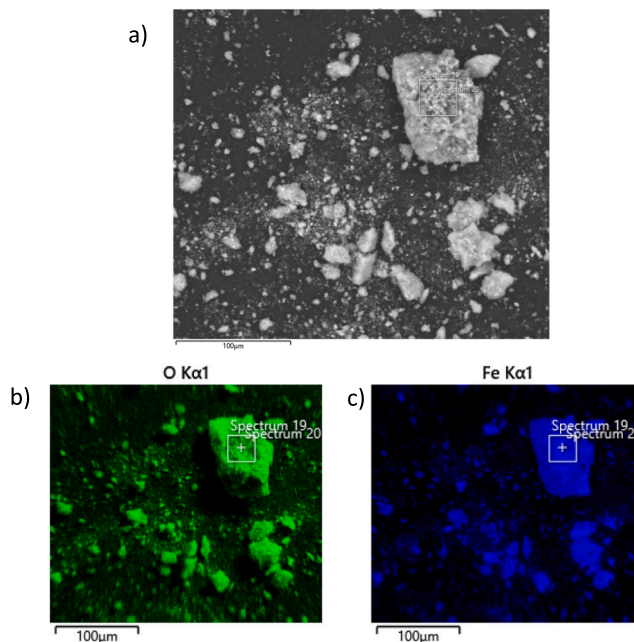


Fig. 2. EDS composition mapping of iron oxide used to simulate the corrosion product in the static examination, a) SEM image of particles, b) oxygen-map and c) iron-map.

**Table 2**  
Area and spot analysis result for sample.

Elements	Areas	Apparent concentration	Wt%	Ratio
Fe	Spectrum 19	22.42	48.79	0.22425
	Spectrum 20	28.18	47.41	0.28181
O	Spectrum 19	24.22	32.95	0.08151
	Spectrum 20	40.01	38.99	0.13464

### 2.3. Theoretical framework

The presented model investigates the relationship between frequency and conductivity in ascertaining the solution's resistance and impedance. Electrical resistance  $R$  is related to the ability of a circuit element to resist the electrical current flow, as seen in Eqs. (1) and (2) [30]. An ideal resistance is characterised by its opposition to electron movement, determined by Ohm's law which have two unique features [18]: 1) the value of an ideal resistor remains unaffected by the alternating current's frequency, and 2) a phase relationship exists between the applied voltage  $V$  and the current  $I$ , which can be defined as:

$$R = V/I \quad (1)$$

The solution material is presumed to be homogeneous and fills the volume defined by two external electrodes. In addition, a visible area  $A$  is formed between the two electrodes with a uniform distance  $d$  between them. By applying an external  $V$  to the solution and a steady  $I$  passes through it, allowing the resistance to be expressed as follows:

$$R = \rho \frac{d}{A} \quad (2)$$

Where  $\rho$  denotes the characteristic electrical resistivity of a material. Impedance, represented by  $Z$ , is the resistance that appears under a potential difference  $E$  against  $I$ , which can be calculated from Eq. (3) [32]. According to Ohm's law, resistance is determined by dividing the potential difference by the current. A distinction exists between impedance  $Z$  and resistance  $R$ , notably, impedance does not require to conformity the previously mentioned two features of ideal resistance. In the EIS test, a sinusoidal alternating current (AC) is employed by frequency  $f$  [16]. Since frequency is in the direction in which oscillations change over time, radial frequency  $\omega$  is an essential parameter to consider and can be obtained as follows:

$$Z = E/I \quad (3)$$

$$\omega = 2\pi f \quad (4)$$

In experimental settings to measure electrochemical impedance, a voltage signal  $E$  with a small amplitude  $E_0$  is typically applied at a given frequency. Consequently, the voltage signal  $E(t)$ , expressed as a function of time  $t$ , has the following form (Eq. (5)) which both voltage and current change over time with AC [27].

$$E(t) = E_0 \sin(\omega t) \quad (5)$$

There is a shift in phase  $\phi$  and a different amplitude  $I_0$  associated with a linear system's response current signal  $I(t)$  when a sinusoidal voltage is applied to the system calculated by Eq. (6).

$$I(t) = I_0 \sin(\omega t + \phi) \quad (6)$$

Hence, an expression analogous to Ohm's law for impedance,  $Z(t)$ , is introduced in Eq. (7).

$$Z(t) = \frac{E(t)}{I(t)} = \frac{E_0 \sin(\omega t)}{I_0 \sin(\omega t + \phi)} = Z_0 \frac{\sin(\omega t)}{\sin(\omega t + \phi)} \quad (7)$$

Fig. 3 indicates the equivalent circuit designed for the experiment,

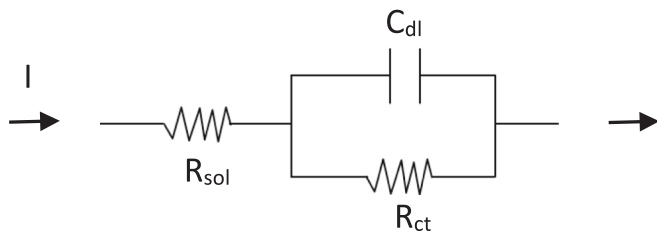


Fig. 3. Simplified equivalent circuit.

aiming to investigate the individual components within the EIS system [50]. The result equivalent circuit indicates a reasonable alignment of the experimental values. Furthermore, given the simplicity of consideration and minimum number of circuit elements, this equivalent circuit was selected as a compromise between these elements and the phenomena likely to occur at the electrode [6]. As a result of the impedance at the highest frequency, the solution resistance is represented as  $R_{sol}$ . The double layer capacitance is symbolised as  $C_{dl}$ , and it includes the sum of distributed capacitance; while  $R_{ct}$  denotes the charge transfer resistance [61]. A further resistance known as the Warburg impedance  $W$  is related to diffusion, which is frequency dependent. The ideal capacitor does not usually exist in the experimental setting, so the constant phase element (CPE) serves as an alternative component to model for non-ideal capacitance.  $W$  in high frequencies is very small, thus it can be omitted from the circuit because diffusing in solution does not have to move very far.

It is possible for a capacitance effect to occur when a solution conducts electricity. Thus, attempting to equate the conductance cell with the solution's resistance become impractical. Due to this, the measurement may be subject to negative effects, such as capacitance effects. A high sinusoidal frequency voltage can lead to quick filling and discharging of capacitor, thus causing the circuit to behave like a short circuit. In other words, this high voltage significantly reduces the negative effects (capacitance effects) on the measurement by stabilising the amplitude and frequency of two electrodes. Accordingly, the current has completely passed through the branch related to the capacitor without being influenced by the charge transfer resistance. Consequently, the only resistance to current flow is the solution resistance.

In terms of equivalent circuit, Euler's Equation is employed to indicate impedance in complex numbers using the exponential form  $Z$ , where phase shift  $\phi$  is a real number (non-zero),  $e$  is the base of the natural logarithm, and  $i$  represents the imaginary unit. In Euler's formula, exponential values are treated as numbers, specifically complex numbers under polar coordinates (Eq. (8)).

$$e^{i\phi} = \cos\phi + i\sin\phi \quad (8)$$

An impedance can also be expressed in complex mathematical format as a combination of "real" and "imaginary" components, as described in Eq. (9).

$$Z = \frac{E}{I} = Z_0 e^{i\phi} = Z_0 (\cos\phi + i\sin\phi) \quad (9)$$

If we define phase angle  $\phi$  as the ratio between imaginary and real impedances at a given radial frequency, it will be:

$$\tan\phi = \frac{e^{i\phi} - e^{-i\phi}}{i(e^{i\phi} + e^{-i\phi})} = \frac{Z'}{Z} \quad (10)$$

Hence, the absolute magnitude of the impedance can be obtained as [28]:

$$|Z| = \sqrt{(Z')^2 + (Z'')^2} \quad (11)$$

The complex impedance of the cell can be presented as  $Z$ , in which [47]

$$Z = R_{sol} + Z_p \quad (12)$$

where  $Z_p$  represents the impedance of the parallel part of the circuit, and its value can be calculated as:

$$\frac{1}{Z_p} = \frac{1}{R_{sol}} + \frac{1}{Z_c} \quad (13)$$

Also,  $Z_c = \frac{1}{j\omega C}$  is the complex impedance for  $C_{dl}$ .

A Nyquist Plot can be formed by plotting the real part ( $Z'$ ) on the X-axis and the imaginary part ( $Z''$ ) on the Y-axis. Another approach for expressing impedance results is known as a Bode plot, which is widely

used in engineering. It comprises two separate logarithmic plots: magnitude versus frequency and phase versus frequency. According to the impedance Bode graph, both series and parallel  $R_{ct}$  and  $C_{dl}$  Circuits have the same characteristic breakpoint frequency (inverse of the characteristic time constant) [32]. Therefore, the impedance of the circuit  $Z$ , is given by the following expressions:

$$Z' = R_{sol} + \frac{R_{ct}}{1 + C_{dl}^2 \cdot \omega^2 \cdot R_{ct}^2} \quad (14)$$

$$Z'' = \frac{-C_{dl} \cdot \omega \cdot i \cdot R_{ct}^2}{1 + C_{dl}^2 \cdot \omega^2 \cdot R_{ct}^2} \quad (15)$$

$$Z = R_{sol} + \frac{R_{ct}}{1 + (\omega \cdot R_{ct} \cdot C_{dl})^2} + \frac{-C_{dl} \cdot \omega \cdot i \cdot R_{ct}^2}{1 + (\omega \cdot R_{ct} \cdot C_{dl})^2} \quad (16)$$

$$|Z| = \sqrt{R_{sol}^2 + \frac{2R_{sol} \cdot R_{ct}}{(\omega \cdot R_{ct} \cdot C_{dl})^2 + 1} + \frac{R_{ct}^2}{(\omega \cdot R_{ct} \cdot C_{dl})^2 + 1}} \quad (17)$$

The phase-angle can be described as [41]:

$$\tan \phi = \frac{Z''}{Z'} = \frac{-\omega \cdot C_{dl} \cdot R_{ct}^2}{R_{sol} + R_{ct} + R_{sol}(\omega \cdot R_{ct} \cdot C_{dl})^2} \quad (18)$$

According to the relationship between  $Z''$  and  $Z'$ , a circle centred on the  $Z'$  axis with a radius of  $R_{ct}/2$  and  $Z' = R_{sol} + R_{ct}/2$  (the distance from the circles' centre to origin) can be described by Eq. (19).

$$(\dot{Z}')^2 = 2R_{sol} \cdot \dot{Z}' + R_{ct} \cdot \dot{Z}' - (\dot{Z}')^2 - R_{sol}^2 - R_{sol} \cdot R_{ct} \quad (19)$$

$$\left[ \dot{Z}' - \left( R_{sol} + \frac{R_{ct}}{2} \right) \right]^2 + (-\dot{Z}')^2 = \left( \frac{R_{ct}}{2} \right)^2$$

#### 2.4. Model description

The exploration of conductivity is a concept partly originated from the Maxwell-Eucken equation, which is used to describe electric conductivity [62]. Eq. (20) shows simple and well-known relation between the conductivity  $K_r$  and volume percentage  $\emptyset$ .

$$K_r = \frac{1 - \emptyset}{1 + \emptyset/2} \quad (20)$$

Through simple theory, this study presents a new perspective on effective problem-solving by employing density  $\rho$  as a parameter to determine the solution's resistivity  $\sigma$ .

$$\rho = \frac{M_T}{V_T} \rightarrow \begin{cases} \frac{M_T}{\rho_T} = \frac{M_p}{\rho_p} + \frac{M_s}{\rho_s} \\ M_p = n \times M_i \end{cases} \quad (21)$$

In Eq. (21), particles mass in solution and total volume of solution ( $M_T$  and  $V_T$ , respectively) can be defined as:

$$V_T = V_p + V_{solvent}, M_T = M_p + M_{solvent} \quad (22)$$

Also, we can obtain the volume percentage by Eq. (23):

$$\emptyset = \left( \frac{M_p}{\rho_p \cdot V_T} \right) \times 100 \quad (23)$$

Finally, the relationship between them is shown in Eq. (24):

$$K_r = \frac{1 - \left( \frac{M_p}{\rho_p \cdot V_T} \right)}{1 + \left( \frac{M_p}{2\rho_p \cdot V_T} \right)} \quad (24)$$

Now, under the assumption there is no chemical reaction in the solution, the relationship between the density of particles in the solution volume is given by:

$$(\rho_p \cdot V_T) = \beta \quad (25)$$

Subsequently, we can derive from transformation that:

$$K_r = \frac{\beta^2 - \beta \cdot M_p}{\beta^2 + \beta(M_p/2)} \quad (26)$$

There is a great deal of complexity in the relationship between electrolyte conductivity and solution resistance. In summary, it is possible to establish a cell constant  $K$  for specifically given temperatures by evaluating the relationship between the solution and particle conductivity where  $K$  is related to the solution conductivity and  $\sigma$  is particles resistivity [53,55]. We modified that relationship to formulate the following model:

$$\sigma = \frac{1}{1 - K_r} \quad (27)$$

The final developed model can be described as the Eq. (28) with empirical function  $\alpha = 1/(0.1^{M_p})$  where  $\sigma_f$  is the solution resistivity. The coefficient represents a parameter in an empirically derived equation that is depended on the variable  $M_p$ . The fitting process involves adjusting the value of  $\sigma_f$  to achieve the optimal alignment between the predicted results and the observed data obtained from experiments. By optimizing the accuracy and applicability of the solution resistivity equation, this fitting process ensures a more robust representation to the investigated system:

$$\sigma_f = \frac{1}{(1 - K_r)(0.1^{M_p})} \quad (28)$$

### 3. Results and discussion

#### 3.1. EIS analysis

EIS measurements are depicted in Fig. 4 on the Nyquist plot, which shows that test 1 exhibits a greater impedance modulus compared to the other tests. The Nyquist plots of the three solutions consist of a large arc in the low-frequency range. This pattern aligns with the complex transfer function of  $Fe_2O_3$ , with confirmation by EDS, through the solution. Also, it is observed that the curve of the circle-fit becomes larger with an increase in concentration content. Hence, the impedance measurement showed significant frequency dispersions as indicated by an inductive response producing a negative impedance [10].

The solution resistance is estimated from the impedance measured in the low-frequency range of the EIS spectrum. Furthermore, the sum of the resistive polarisation ( $R_{ct}$ ) and the solution resistance ( $R_{sol}$ ) is calculated from the impedance measured in the high-frequency range of the EIS spectrum. Bode graphs in Fig. 4 illustrate that the measured impedance data and resistance-related parameters like resonant frequency and cut-off frequency. The impedance graphs demonstrate typical CPE characteristics in the low-frequency range, almost at the critical frequency. Low frequencies appear to exhibit a change in behavior as a function of concentration. As expected, the lowest solution resistance was observed in test 3.

A distinctive capacitive behavior is evident in test 1 with lower phase angles, even in the low-frequency domain compared with the other tests, where an increase in electrolyte concentration resulted in a shift in the characteristic frequency of the electrolyte solution. As a result, the phase plot shifts to a higher frequency with an increase in electrolyte solution concentration [27]. Further, the phase angle can be attributed to the association of a capacitive time constant related to dielectric properties. An unfinished arc in the Nyquist diagram corresponds to phase angle-log frequency in the Bode diagram at lower frequency range, which is linked to mass transport [40].

Furthermore, Fig. 4 shows that the equivalent circuit is a perfect fit, as calibrated results for the experimental data for this frequency range

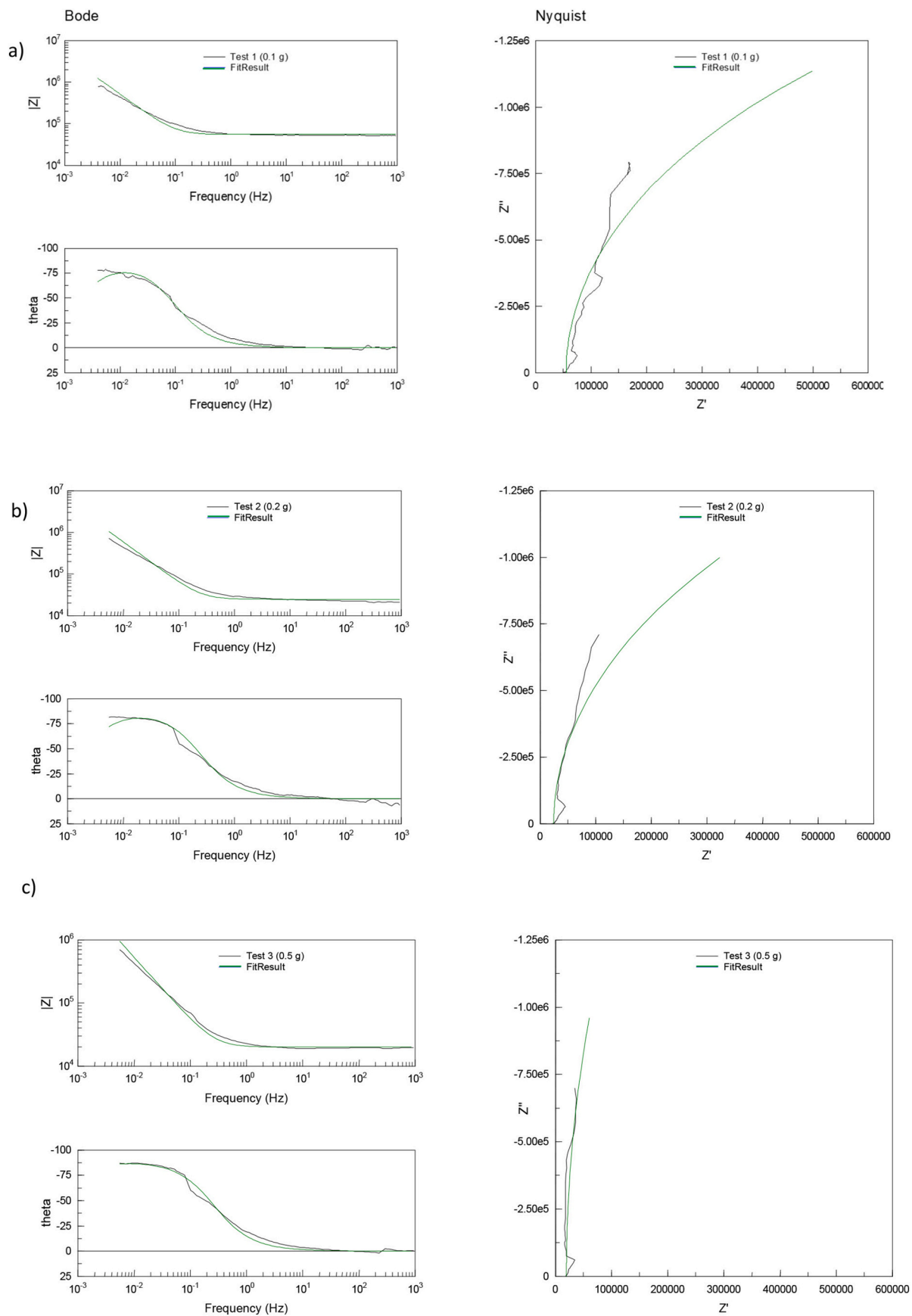


Fig. 4. EIS Nyquist and Bode plots of corrosive particles ( $\text{Fe}_2\text{O}_3$ ) in 900 ml of distilled water with the fitted result (calibrated results), a) test 1 (0.1 g), b) test 2 (0.2 g), and c) test 3 (0.5 g).

confirm the equivalent circuits' validity. The regression coefficients for all tests exceed 0.95, indicating high confidence in the fitted model results between the real and imaginary data (Table 3). Therefore, the model can predict the long-term effect of this relation reasonably.

An equivalent circuit representing the electrochemical parameters of the solutions is detailed in Table 4. In test 1, the  $R_{sol}$  value of the solution exceeds that of the solution in test 3 by more than two times, while the  $R_{ct}$  value is approximately ten times higher than that of the solution in test 3. Consequently, reduction of the concentration enhances the solution resistance. The  $C_{dl}$  is very small across all tests, making it negligible. The low  $R_{ct}$  values can be attributed to a decrement in the number of particles within the solution, which means the solution resistance decreases as  $Fe_2O_3$  concentration increases.

### 3.2. Root mean square error (RMSE)

The Root Mean Square Error (RMSE) have been employed as the utilised criterion to represent the differences between the predicted values (P) derived from the model and the corresponding experimental results (A). Using Eq. (29), it is possible to determine how closely the predictions match the actual outcomes showed in Table 4. A lower percentage of RMSE suggests a closer agreement with the actual data, indicating good performance in predicting the solution resistance at high concentration.

$$\%RMSE = \frac{\sqrt{(P_n - A_n)^2}}{(Max A - Min A)} \times 100 \quad (29)$$

### 3.3. Model results validation

All relevant parameters have been accurately measured and integrated into the mathematical formulations of the models, as shown in Table 5. The model relies on three assumptions: firstly, the a high solvent resistivity is present. Distilled water, known for its low conductivity characteristics, has been employed in the experimentation process. Secondly, the mobility of charged particles (ions) within the solution is uniform. Thirdly, the temperature was maintained at a constant level throughout the entire testing period. In this study, the mass of particles is considered as the independent variable, where it directly influences the study's outcome. On the other hand, the total volume and total mass are considered dependent variables, and changes in the mass of particles influence them.

In Fig. 5, the analytical model from Eq. (28) was compared with the experimental results relating to concentration. The model exhibited a close alignment with the experimental findings. Based on the experimental results, the mathematical model has been validated as predicted by Eq. (28), demonstrating the effectiveness of logarithmic equation in characterising its specific behavior. A regression coefficient of 0.78 indicates a relatively strong correlation between the studied variables and the applied model, demonstrating the reliability of this representation. Furthermore, these results establish an important benchmark, particularly in the context of particle concentration analysis. It serves as a benchmark for future experimental endeavors in similar contexts, delineating the level of accuracy achievable with this method. On the other hand, the graphical analysis illustrates a decreasing trend in resistivity as concentration increases which aligns well with the model's predictions. This correlation is supported by a low RMSE which is essential for validating the model's performance. However, there are

**Table 3**  
Circle fitting of Nyquist plots in experimental analysis.

Tests	Equation	Coefficient regression
1	$y = 536853\ln(x) - 6E+06$	$R^2 = 0.9825$
2	$y = 392625\ln(x) - 4E+06$	$R^2 = 0.9891$
3	$y = 965005\ln(x) - 1E+07$	$R^2 = 0.9517$

**Table 4**

Resistance of the solution used in three different experimental tests.

Name	Concentration (g)	$R_{sol}$ (ohms. $cm^2$ )	$R_{ct}$ (ohms. $cm^2$ )	$C_{dl}$ (F)	RMSE (%)
Test 1	0.1	55,363	2,958,100	0.000029602	34.8
Test 2	0.2	24,740	3,641,400	0.000026229	6.7
Test 3	0.5	20,026	22,634,000	0.000029649	4.5

recognisable discrepancies between the model's predictions and the experimental results at low concentrations. These discrepancies can be attributed to the influence of suspended particles within the solution during the testing period.

The solution conductivity change expected to be independent of particle size. However, the result suggest the particle concentration as a critical parameter influencing conductivity (also agreed by Rong and Feng [62]). Resistance demonstrated a significant decline from 55,363  $\Omega.cm^2$  to 24,740  $\Omega.cm^2$  as the concentration increased from 0.1 g to 0.2 g. When the particle concentration exceeds 0.2 g, the resistance change occurs (about 4714  $\Omega.cm^2$  decreases in solution with concentration 0.5 g). This pattern indicated maximum saturation of insoluble particles at this concentration within specific volume fluid, suggesting a point beyond which no further dissolution can take place.

## 4. Conclusion

A mathematical approach to calculate solution conductivity was proposed to model of the solution resistance by analysing the particles mass. The analysis revealed that there is a direct correlation between the particles concentration and solution resistance containing  $Fe_2O_3$ . The modelled results indicated that with the addition of particles to the system, the effective conductivity increases, leading to a decrease in solution resistance. Moreover, it was found that a characteristic frequency, which can be derived directly from the Nyquist plot through fitting, can be used to evaluate the solution structure. The characteristic frequency would increase with increasing particle concentrations in solution at a given electrolyte concentration. In this aspect, it is also beneficial to conduct further studies incorporating temperature and diffusion considerations to provide a theoretical prediction for refining the empirical coefficient  $\alpha$ . Accounting for these factors enables a more comprehensive understanding of the relationship between the coefficient  $\alpha$  and its dependence on temperature and diffusion.

It has been found that the resistance in 0.1 g concentration is 55,363  $\Omega.cm^2$  declined in non-linear manner to 21,633  $\Omega.cm^2$  in concentration of 0.2 g. Then solution conductivity is influenced by the saturation of iron oxide (after concentration of 0.2 g), resulting in the less contribution of charged particles. In a low-concentration solution (test 1), there are fewer particles available to carry electric current, resulting in elevated resistance. The combination of these factors plays an important role in altering the electrical characteristics of the solution. Specifically, a reduced particle count directly correlates with fewer conductive pathways, which increases the resistance of the solution. Additionally, the reduction in particle mass indicates a lower availability of conductive material, further contributing to the increase in resistivity. However, a portion of the particles larger than 0.2 g may have sedimented, resulting in a lower contribution to the change in resistance. As a result of this sedimentation process, particles are effectively removed from the solution's active volume, thereby reducing their impact on the overall conductivity of the solution and gradually decreases the resistance of solution.

## CRediT authorship contribution statement

**Nima Ikani:** Conceptualization, Data curation, Formal analysis, Investigation, Methodology, Validation, Writing – original draft. **Jaana**

**Table 5**  
Resistance for solution in three different tests according to model.

	$M_p$ (g)	$\rho_p$ (g/cm <sup>3</sup> )	$V_p$ (cm <sup>3</sup> )	$V_s$ (cm <sup>3</sup> )	$V_T$ (cm <sup>3</sup> )	B	1- $K_r$	$\alpha$	$\sigma_f$
Model	0.1	5.7	0.0175438	900	900.01754	5130.1	0.00002924	1.2589	43,056
	0.2	5.7	0.0350877	900	900.03508	5130.2	0.00005848	1.4466	27,103
	0.5	5.7	0.0877192	900	900.08771	5130.5	0.00014618	2.9273	21,633

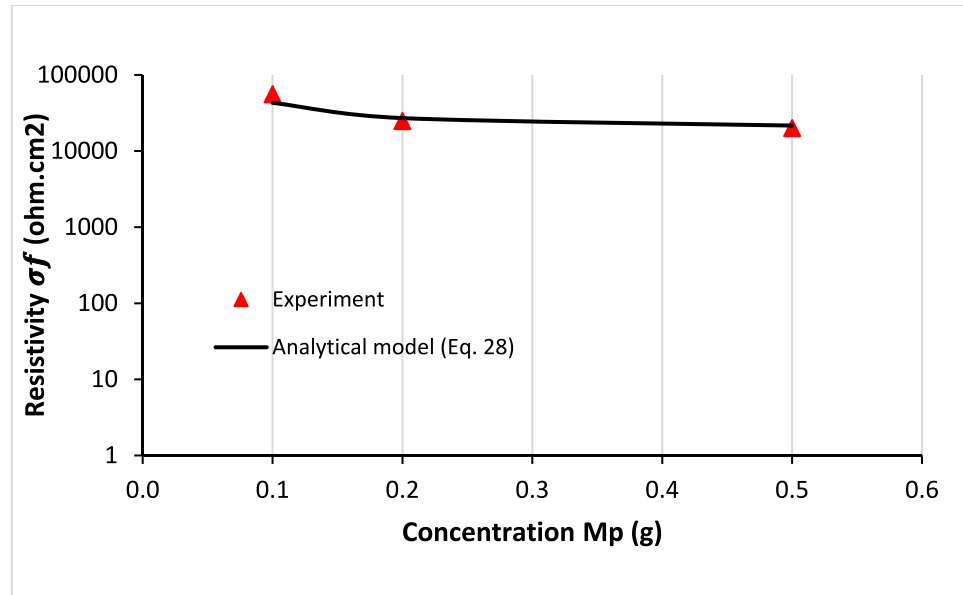


**Fig. 5.** Comparison of analytical model and experiment results.

**H. Pu:** Conceptualization, Data curation, Formal analysis, Funding acquisition, Investigation, Methodology, Project administration, Resources, Supervision, Validation, Writing – review & editing. **Kavian Cooke:** Conceptualization, Data curation, Methodology, Supervision, Writing – review & editing.

#### Declaration of Competing Interest

The authors declare no conflict of interest.

#### Data availability

Data will be made available on request.

#### References

- [1] C.L. Alexander, M.E. Orazem, Indirect electrochemical impedance spectroscopy for corrosion detection in external post-tensioned tendons: 1. Proof of concept, *Corros. Sci.* 164 (2020), 108331.
- [2] W. Badawy, F. Al-Kharafi, Corrosion and passivation behaviors of molybdenum in aqueous solutions of different pH, *Electrochim. Acta* 44 (1998) 693–702.
- [3] N. Balasubramanian, S. Prabhu, N. Sakthivel, R. Ramesh, S.A. Kumar, P. Anbarasan, Electrochemical performance of Fe<sub>2</sub>O<sub>3</sub>@ PPy nanocomposite as an effective electrode material for supercapacitor, *ECS J. Solid State Sci. Technol.* 11 (2022), 091001.
- [4] J. Bessone, D. Salinas, C. Mayer, M. Ebert, W. Lorenz, An EIS study of aluminium barrier-type oxide films formed in different media, *Electrochim. Acta* 37 (1992) 2283–2290.
- [5] P. Bommersbach, C. Alemany-Dumont, J.-P. Millet, B. Normand, Formation and behaviour study of an environment-friendly corrosion inhibitor by electrochemical methods, *Electrochim. Acta* 51 (2005) 1076–1084.
- [6] M. Cardoso, S. Amaral, E. Martini, Temperature effect in the corrosion resistance of Ni–Fe–Cr alloy in chloride medium, *Corros. Sci.* 50 (2008) 2429–2436.
- [7] F. Ciucci, Modeling electrochemical impedance spectroscopy, *Curr. Opin. Electrochem.* 13 (2019) 132–139.
- [8] L. Colla, L. Fedele, M. Scattolini, S. Bobbo, Water-based Fe<sub>2</sub>O<sub>3</sub> nanofluid characterization: thermal conductivity and viscosity measurements and correlation, *Adv. Mech. Eng.* 4 (2012), 674947.
- [9] K. Dai, S. Li, P. Hu, N. Jiang, D. Wang, Effect of outer rust layer on cathodic protection and corrosion behavior of high-strength wire hangers with sheath crack in marine rainfall environment, *Case Stud. Construct. Mater.* 18 (2023), e02043.
- [10] G. Duan, L. Yang, S. Liao, C. Zhang, X. Lu, Y. Yang, B. Zhang, Y. Wei, T. Zhang, B. Yu, Designing for the chemical conversion coating with high corrosion resistance and low electrical contact resistance on AZ91D magnesium alloy, *Corros. Sci.* 135 (2018) 197–206.
- [11] R. Duarte, A. Castela, R. Neves, L. Freire, M. Montemor, Corrosion behavior of stainless steel rebars embedded in concrete: an electrochemical impedance spectroscopy study, *Electrochim. Acta* 124 (2014) 218–224.
- [12] V. Encinas-Sánchez, M. De Miguel, M. Lasanta, G. García-Martín, F. Pérez, Electrochemical impedance spectroscopy (EIS): an efficient technique for monitoring corrosion processes in molten salt environments in CSP applications, *Sol. Energy Mater. Sol. Cells* 191 (2019) 157–163.
- [13] G. Falzone, M. Balonis, D. Bentz, S. Jones, G. Sant, Anion capture and exchange by functional coatings: new routes to mitigate steel corrosion in concrete infrastructure, *Cem. Concr. Res.* 101 (2017) 82–92.
- [14] E. Ferrara, L. Callegaro, F. Durbiano, Optimal frequency range for the measurement of AC conductivity in aqueous solutions, in: *Proceedings of the 17th IEEE Instrumentation and Measurement Technology Conference [Cat. No. 00CH37066]*, IEEE, 2000, pp. 775–779.
- [15] L. Freire, M. Carmezim, M. Ferreira, M. Montemor, The electrochemical behaviour of stainless steel AISI 304 in alkaline solutions with different pH in the presence of chlorides, *Electrochim. Acta* 56 (2011) 5280–5289.
- [16] M.H. Garrido, M. Pritzker, EIS and statistical analysis of copper electrodeposition accounting for multi-component transport and reactions, *J. Electroanal. Chem.* 594 (2006) 118–132.
- [17] B. Grysakowski, J. Jasielc, B. Wierzbna, T. Sokalski, A. Lewenstam, M. Danielewski, Electrochemical impedance spectroscopy (EIS) of ion sensors: direct modeling and inverse problem solving using the Nernst–Planck–Poisson (NPP) model and the HGS (FP) optimization strategy, *J. Electroanal. Chem.* 662 (2011) 143–149.
- [18] L.D. Ha, K. Park, B.-Y. Chang, S. Hwang, Implementation of second-generation fourier transform electrochemical impedance spectroscopy with commercial potentiostat and application to time-resolved electrochemical impedance spectroscopy, *Anal. Chem.* 91 (2019) 14208–14213.
- [19] X. He, M.H. Azarian, M.G. Pecht, Analysis of the kinetics of electrochemical migration on printed circuit boards using Nernst–Planck transport equation, *Electrochim. Acta* 142 (2014) 1–10.
- [20] T. Holm, M. Ingdal, E.V. Fanavoll, S. Sunde, F. Seland, D.A. Harrington, Mass-transport impedance at channel electrodes: accurate and approximate solutions, *Electrochim. Acta* 202 (2016) 84–89.

- [21] Y. Hoshi, T. Koike, H. Tokieda, I. Shitanda, M. Itagaki, Y. Kato, Non-contact measurement to detect steel rebar corrosion in reinforced concrete by electrochemical impedance spectroscopy, *J. Electrochem. Soc.* 166 (2019) C3316.
- [22] B.-R. Hou, J.-L. Zhang, H.-Y. Sun, Y. Li, B. Xiang, Corrosion of C-Mn steel in simulated tidal and immersion zones, *Br. Corros. J.* 36 (2001) 310–312.
- [23] X. Hou, Q. Ren, Y. Yang, X. Cao, J. Hu, C. Zhang, H. Deng, D. Yu, K. Li, W. Lan, Effect of temperature on the electrochemical pitting corrosion behavior of 316L stainless steel in chloride-containing MDEA solution, *J. Nat. Gas Sci. Eng.* 86 (2021), 103718.
- [24] J. Hu, S.A. Cao, J. Xie, EIS study on the corrosion behavior of rusted carbon steel in 3% NaCl solution, *Anti-Corros. Methods Mater.* 60 (2013) 100–105.
- [25] J. Huang, Diffusion impedance of electroactive materials, electrolytic solutions and porous electrodes: Warburg impedance and beyond, *Electrochim. Acta* 281 (2018) 170–188.
- [26] J. Huang, Y. Gao, J. Luo, S. Wang, C. Li, S. Chen, J. Zhang, Editors' choice—review—impedance response of porous electrodes: theoretical framework, physical models and applications, *J. Electrochem. Soc.* 167 (2020), 166503.
- [27] Q. Huang, Q. Luo, Z. Chen, L. Yao, P. Fu, Z. Lin, The effect of electrolyte concentration on electrochemical impedance for evaluating polysulfone membranes, *Environ. Sci. Water Res. Technol.* 4 (2018) 1145–1151.
- [28] N. Ida, N. Meyendorf, *Handbook of Advanced Nondestructive Evaluation*, Springer International Publishing Cham, Switzerland, 2019.
- [29] N. Ikani, J.H. Pu, T. Taha, P.R. Hanmaiahgarib, N. Penna, Bursting phenomenon created by bridge piers group in open channel flow, *Environ. Fluid Mech.* (2023) 1–16.
- [30] S. Irawan, K. Permatasari, R. Bayuaji, Effect of density and resistivity measurement for foam flooding propagation in static condition, in: *IOP Conference Series: Materials Science and Engineering*, IOP Publishing, 2017, p. 012031.
- [31] M.S. Islam, M. Sakairi, Corrosion inhibition of mild steel by metal cations in high pH simulated fresh water at different temperatures, *Corros. Sci.* 153 (2019) 100–108.
- [32] M. Itagaki, S. Suzuki, I. Shitanda, K. Watanabe, Electrochemical impedance and complex capacitance to interpret electrochemical capacitor, *Electrochemistry* 75 (2007) 649–655.
- [33] J. Jamnik, J. Maier, S. Pejovnik, A powerful electrical network model for the impedance of mixed conductors, *Electrochim. Acta* 44 (1999) 4139–4145.
- [34] M. Jia, W. Zhang, X. Cai, X. Zhan, L. Hou, C. Yuan, Z. Guo, Re-understanding the galvanostatic intermittent titration technique: pitfalls in evaluation of diffusion coefficients and rational suggestions, *J. Power Sources* 543 (2022), 231843.
- [35] P. Kritzer, N. Boukis, E. Dinjus, Factors controlling corrosion in high-temperature aqueous solutions: a contribution to the dissociation and solubility data influencing corrosion processes, *J. Supercrit. Fluids* 15 (1999) 205–227.
- [36] W. Kuczma, M. Danielewski, A. Lewenstam, EIS simulations for ion-selective site-based membranes by a numerical solution of the coupled Nernst–Planck–Poisson equations, *Electrochem. Commun.* 8 (2006) 416–420.
- [37] S. Kulkarni, C. Lokhande, Structural, optical, electrical and dielectrical properties of electrosynthesized nanocrystalline iron oxide thin films, *Mater. Chem. Phys.* 82 (2003) 151–156.
- [38] P. Lan, T. Liu, X. Ji, S. Cheng, Charge storage behavior and reaction mechanism of  $\alpha$ -Fe<sub>2</sub>O<sub>3</sub> as anodes for aqueous batteries, *J. Alloys Compd.* 859 (2021), 157789.
- [39] L. Landa-Ruiz, M.A. Baltazar-Zamora, J. Bosch, J. Ressa, G. Santiago-Hurtado, V. M. Moreno-Landeros, S. Márquez-Montero, C.T. Méndez, A. Borunda, C.A. Juárez-Alvarado, Electrochemical corrosion of galvanized steel in binary sustainable concrete made with sugar cane bagasse ash (SCBA) and silica fume (SF) exposed to sulfates, *Appl. Sci.* 11 (2021) 2133.
- [40] N.O. Laschuk, E.B. Easton, O.V. Zenkina, Reducing the resistance for the use of electrochemical impedance spectroscopy analysis in materials chemistry, *RSC Adv.* 11 (2021) 27925–27936.
- [41] A. Leasia, *Electrochemical Impedance Spectroscopy and its Applications*, Springer, 2002.
- [42] Y. Leng, J. Zhang, S. Cheng, Z. Ye, A mathematical model for electrochemical impedance spectroscopy (EIS) of metal hydride electrodes, *Electrochim. Acta* 43 (1998) 1945–1949.
- [43] S. Li, Z. Jin, B. Pang, J. Li, Durability performance of an RC beam under real marine all corrosion zones exposure for 7 years, *Case Stud. Construct. Mater.* 17 (2022), e01516.
- [44] L. Liu, Y. Li, C. Zeng, F. Wang, Electrochemical impedance spectroscopy (EIS) studies of the corrosion of pure Fe and Cr at 600 C under solid NaCl deposit in water vapor, *Electrochim. Acta* 51 (2006) 4736–4743.
- [45] P. Liu, W. Zhang, Y. Zhang, X. Dai, F. Wu, Study on electrochemical impedance spectrum of C-LiFePO<sub>4</sub> power battery, in: *IOP Conference Series: Materials Science and Engineering*, IOP Publishing, 2018, p. 032089.
- [46] S. Liu, H. Sun, L. Sun, H. Fan, Effects of pH and Cl<sup>-</sup> concentration on corrosion behavior of the galvanized steel in simulated rust layer solution, *Corros. Sci.* 65 (2012) 520–527.
- [47] Z. Lukács, T. Kristóf, A generalized model of the equivalent circuits in the electrochemical impedance spectroscopy, *Electrochim. Acta* 363 (2020), 137199.
- [48] I. Lukovits, E. Kalman, F. Zucchi, Corrosion inhibitors—correlation between electronic structure and efficiency, *Corrosion* 57 (2001) 3–8.
- [49] H. Ma, C. Yang, G. Li, W. Guo, S. Chen, J. Luo, Influence of nitrate and chloride ions on the corrosion of iron, *Corrosion* 59 (2003).
- [50] H.S. Magar, R.Y. Hassan, A. Mulchandani, Electrochemical impedance spectroscopy (EIS): principles, construction, and biosensing applications, *Sensors* 21 (2021) 6578.
- [51] A. Malik, P.M. Kutty, N.A. Siddiqi, I.N. Andijani, S. Ahmed, The influence of pH and chloride concentration on the corrosion behaviour of AISI 316L steel in aqueous solutions, *Corros. Sci.* 33 (1992) 1809–1827.
- [52] K.J. McKenzie, F. Marken, Direct electrochemistry of nanoparticulate Fe<sub>2</sub>O<sub>3</sub> in aqueous solution and adsorbed onto tin-doped indium oxide, *Pure Appl. Chem.* 73 (2001) 1885–1894.
- [53] M.D. Merrill, B.E. Logan, Electrolyte effects on hydrogen evolution and solution resistance in microbial electrolysis cells, *J. Power Sources* 191 (2009) 203–208.
- [54] P. Mishra, D. Yavas, A.F. Bastawros, K.R. Hebert, Electrochemical impedance spectroscopy analysis of corrosion product layer formation on pipeline steel, *Electrochim. Acta* 346 (2020), 136232.
- [55] Z. Morón, Investigations of van der Pauw method applied for measuring electrical conductivity of electrolyte solutions: measurement of electrolytic conductivity, *Measurement* 33 (2003) 281–290.
- [56] G. Murphy, D. Caudle, Mathematical theory of electrochemical demineralization in flowing systems, *Electrochim. Acta* 12 (1967) 1655–1664.
- [57] A. Nasser-Eddine, B. Huard, J.-D. Gabano, T. Poinot, A two steps method for electrochemical impedance modeling using fractional order system in time and frequency domains, *Control. Eng. Pract.* 86 (2019) 96–104.
- [58] I.M. Pateli, A.P. Abbott, G.R. Jenkin, J.M. Hartley, Electrochemical oxidation as alternative for dissolution of metal oxides in deep eutectic solvents, *Green Chem.* 22 (2020) 8360–8368.
- [59] N. Priyantha, P. Jayaweera, A. Sanjurjo, K. Lau, F. Lu, K. Krist, Corrosion-resistant metallic coatings for applications in highly aggressive environments, *Surf. Coat. Technol.* 163 (2003) 31–36.
- [60] W. Rahmanto, R. Nuryanto, Corrosion rate of copper and iron in seawater based on resistance measurement, *J. Coast. Developm.* 5 (2002) 67–74.
- [61] U. Rammelt, G. Reinhard, Application of electrochemical impedance spectroscopy (EIS) for characterizing the corrosion-protective performance of organic coatings on metals, *Prog. Org. Coat.* 21 (1992) 205–226.
- [62] Z. Rong, Q. Feng, How insoluble particles affect the solutions' conductivity: a theory and the test in NaCl and chitosan solutions, *J. Phys. Chem. B* 115 (2011) 12816–12821.
- [63] A. Sander, B. Berghult, E. Ahlberg, A.E. Broo, E.L. Johansson, T. Hedberg, Iron corrosion in drinking water distribution systems—surface complexation aspects, *Corros. Sci.* 39 (1997) 77–93.
- [64] J. Scully, S. Hensley, Lifetime prediction for organic coatings on steel and a magnesium alloy using electrochemical impedance methods, *Corrosion* 50 (1994) 705–716.
- [65] E.E. Stansbury, R.A. Buchanan, *Fundamentals of electrochemical corrosion*, ASM Intern (2000).
- [66] M. Stefanoni, Z. Zhang, U.M. Angst, B. Elsener, The kinetic competition between transport and oxidation of ferrous ions governs precipitation of corrosion products in carbonated concrete, *RILEM Techn. Lett.* 3 (2018) 8–16.
- [67] Z. Tang, Q.-A. Huang, Y.-J. Wang, F. Zhang, W. Li, A. Li, L. Zhang, J. Zhang, Recent progress in the use of electrochemical impedance spectroscopy for the measurement, monitoring, diagnosis and optimization of proton exchange membrane fuel cell performance, *J. Power Sources* 468 (2020), 228361.
- [68] A.E. Tudose, I. Demetrescu, F. Golgovici, M. Fulger, Oxidation behavior of an austenitic steel (Fe, Cr and Ni), the 310 H, in a deaerated supercritical water static system, *Metals* 11 (2021) 571.
- [69] S. Wang, J. Zhang, O. Gharbi, V. Vivier, M. Gao, M.E. Orazem, Electrochemical impedance spectroscopy, *Nat. Rev. Methods Prim.* 1 (2021) 41.
- [70] D.-H. Xia, C.-M. Deng, D. Macdonald, S. Jamali, D. Mills, J.-L. Luo, M.G. Strelb, M. Amiri, W. Jin, S. Song, Electrochemical measurements used for assessment of corrosion and protection of metallic materials in the field: A critical review, *J. Mater. Sci. Technol.* 112 (2022) 151–183.
- [71] W. Yuan, A. Guo, W. Yuan, H. Li, Shaking table tests of coastal bridge piers with different levels of corrosion damage caused by chloride penetration, *Constr. Build. Mater.* 173 (2018) 160–171.
- [72] J. Zhao, Y. Lin, X. Li, Q. Meng, Experimental study on the cyclic behavior of reinforced concrete bridge piers with non-uniform corrosion, *Structures* (2021) 999–1006. Elsevier.
- [73] J. Zhao, Y. Liu, X. Yang, X. He, L. Wang, D. Xiong, Y. Gu, Corrosion behavior of pipeline steel in oilfield produced water under dynamic corrosion system, *J. Wuhan Univ. Technol. Mater. Sci. Ed.* 37 (2022) 677–691.
- [74] H. Zhou, S. Chen, Y. Du, Z. Lin, X. Liang, J. Liu, F. Xing, Field test of a reinforced concrete bridge under marine environmental corrosion, *Eng. Fail. Anal.* 115 (2020), 104669.
- [75] S. Ziemiak, M. Hanson, Corrosion behavior of 304 stainless steel in high temperature, hydrogenated water, *Corros. Sci.* 44 (2002) 2209–2230.
- [76] L. Su, X. Liao, Z. Huang, A theoretical study on resistance of electrolytic solution: Measurement of electrolytic conductivity, *Results Phys.* 13 (2019) 102274.